Electronic Supplementary Material (ESI) for Materials Chemistry Frontiers.

Supporting Information

In situ-fabricated p-Co_3O_4@n-ZnO surface heterojunction photocatalyst for solar-to-fuel conversion of CO_2

Qiuyan Wang, ‡[a] Kui Chen, ‡[a] Shuhui Wang,[b] Daheng Jiang,[a] Changqiu Ma,[a] Lixin Zhu*[c] and Xiaoliang Xu*[a]

[a] Key Laboratory of Strongly-Coupled Quantum Matter Physics, Chinese Academy of Sciences, School of Physical Sciences, University of Science and Technology of China, Hefei, Anhui 230026, PR China.

[b] Fujian Key Laboratory of Agricultural Information Sensoring Technology, College of Mechanical and Electrical Engineering, Fujian Agriculture and Forestry University, Fuzhou, Fujian 350002, PR China.

[c] Department of General Surgery and Central Laboratory, the First Affiliated Hospital of Anhui Medical University, Hefei, Anhui 230022, PR China.

‡ These authors contributed equally to this work.

*Corresponding authors: Lixin Zhu (zhulixin@ahmu.edu.cn)

Xiaoliang Xu (xlxu@ustc.edu.cn)

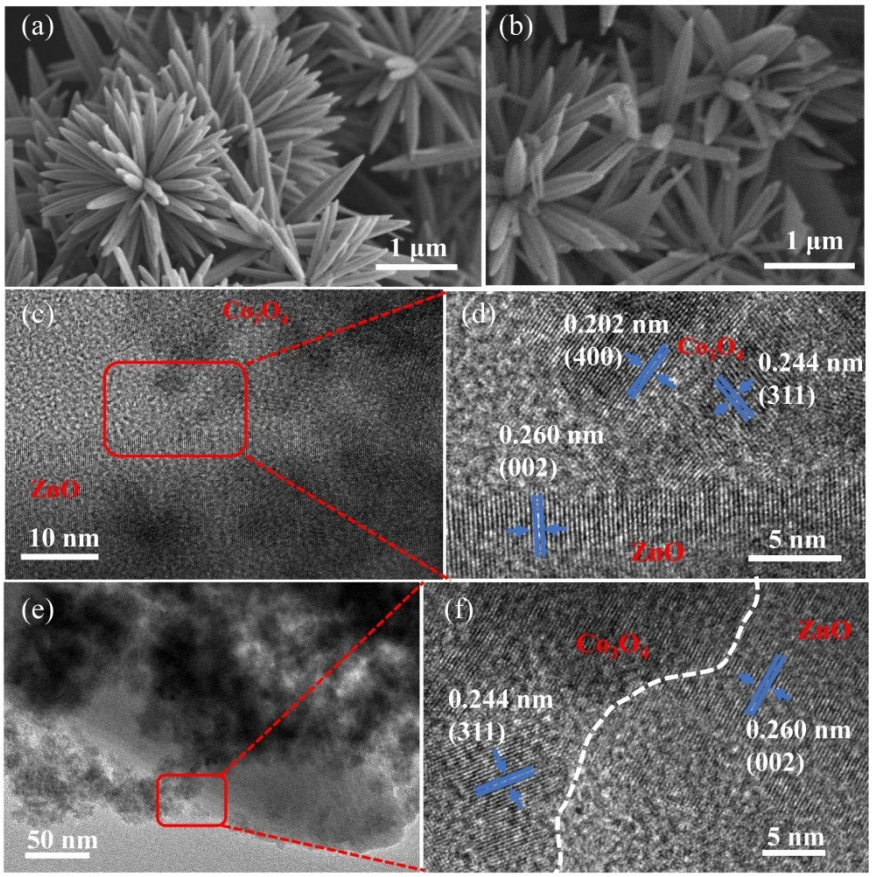

Fig. S1 (a, b) The SEM images of ZnO, (c-f) the HRTEM images of Co_3O_4@ZnO.

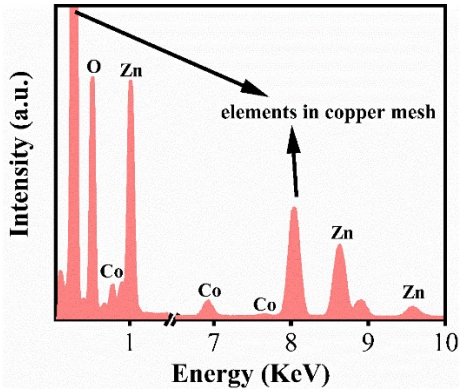

Fig. S2 Corresponding element energy spectrum of Fig. 1f.

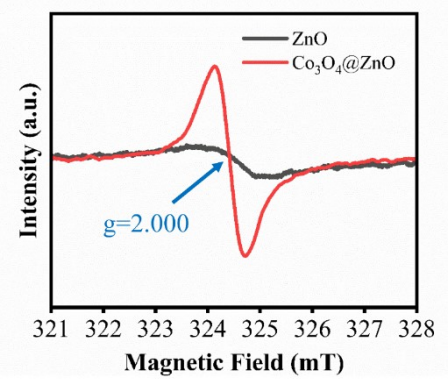

Fig. S3 EPR spectra of ZnO and Co_3O_4@ZnO.

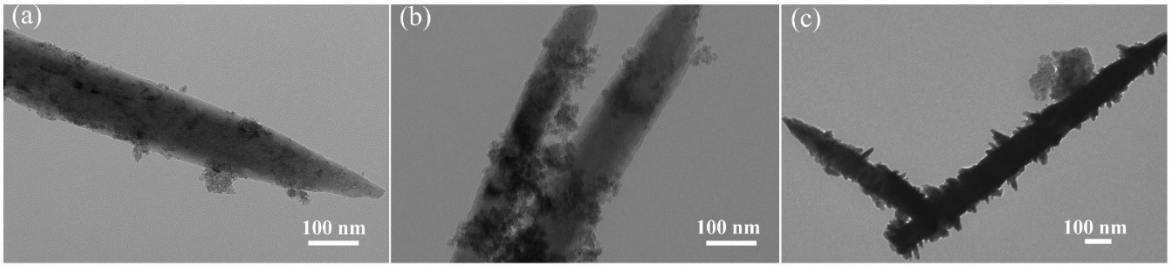

Fig. S4 The TEM images of (a) 0.3-Co_3O_4@ZnO, (b) 0.6-Co_3O_4@ZnO, and (c) 0.9-Co_3O_4@ZnO.

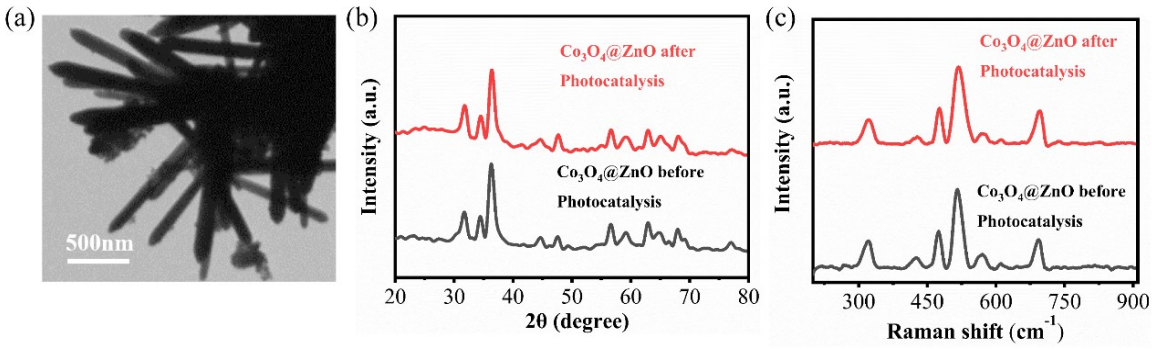

Fig. S5 (a) TEM, (b) XRD and (c) Raman characterizations for Co_3O_4@ZnO after 30 h photoreduction CO_2 reaction.

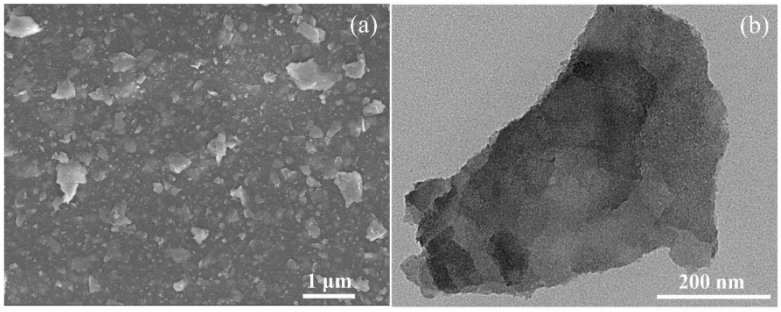

Fig. S6 (a) SEM and (b) TEM images of Co_3O_4.

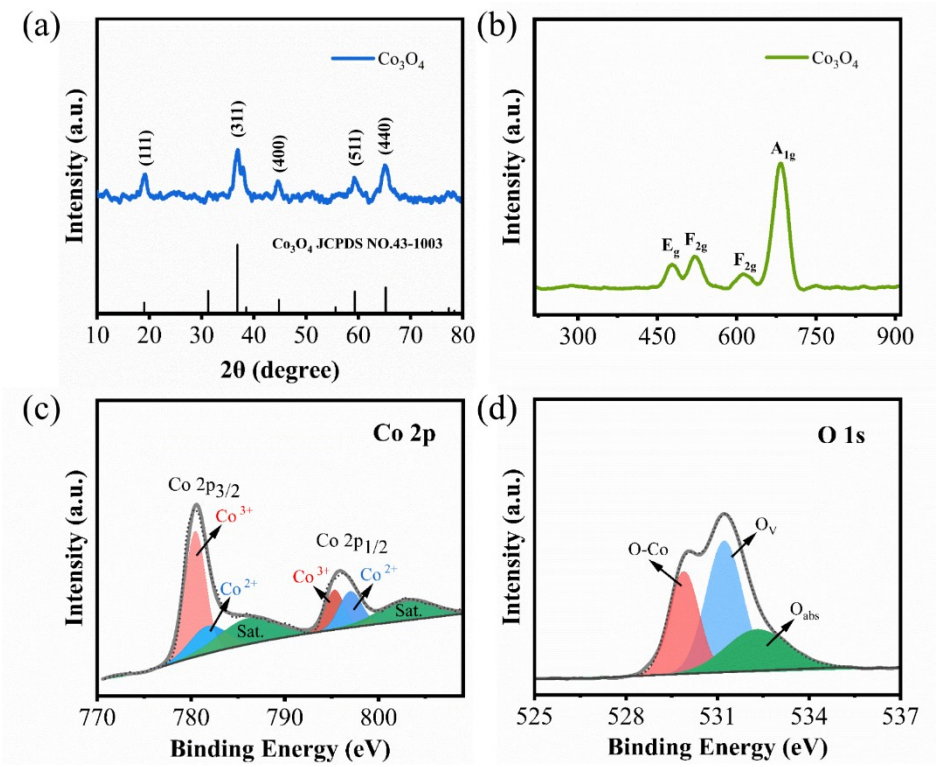

Fig. S7 (a) XRD pattern, (b) Raman spectrum of Co_3O_4. High-resolution XPS spectra of Co_3O_4: (c) Co 2p and (d) O 1s.

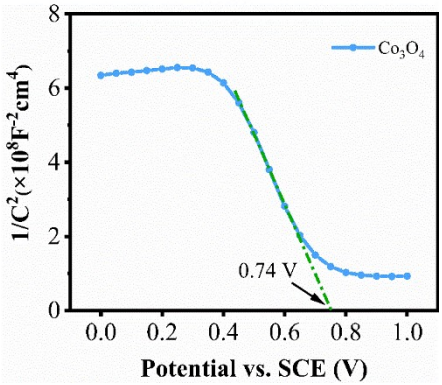

Fig. S8 Mott-Schottky plot of Co_3O_4.

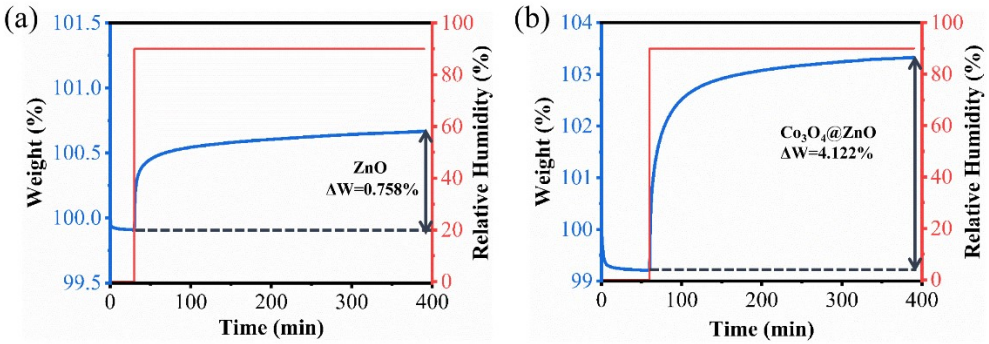

Fig. S9 Dynamic H_2O vapor adsorption isotherms of (a) ZnO, and (b) Co_3O_4@ZnO.

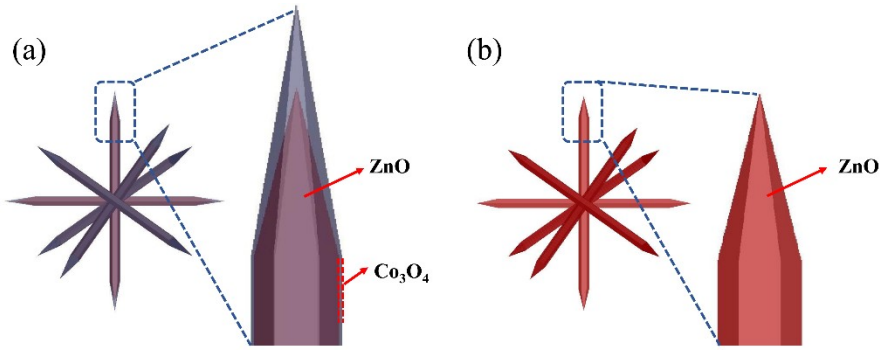

Fig. S10 The models of (a) Co_3O_4@ZnO and (b) ZnO for FDTD simulations.

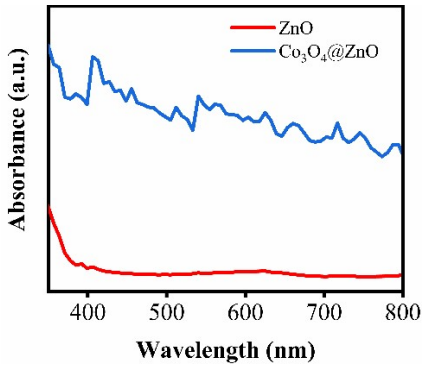

Fig. S11 The simulated UV−vis absorption spectra of ZnO and Co_3O_4@ZnO.

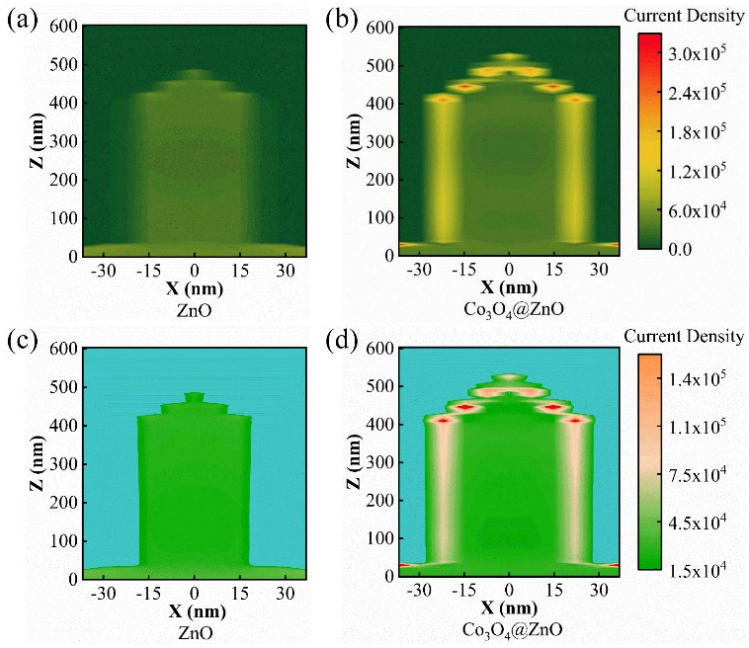

Fig. S12 The simulations of photocurrent density distribution of ZnO and Co_3O_4@ZnO under light irradiation at (a, b) 550 nm and (c, d) 700 nm.

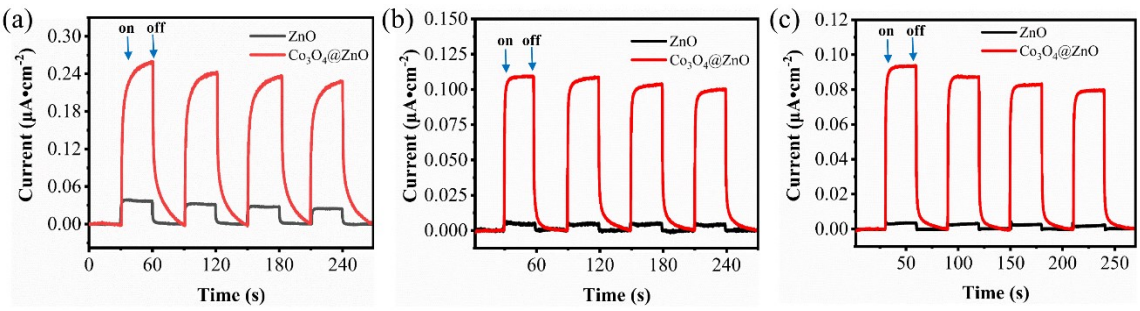

Fig. S13 The single-band I-t of ZnO and Co_3O_4@ZnO under light irradiation at (a)

400, (b) 550, and (c) 700 nm.

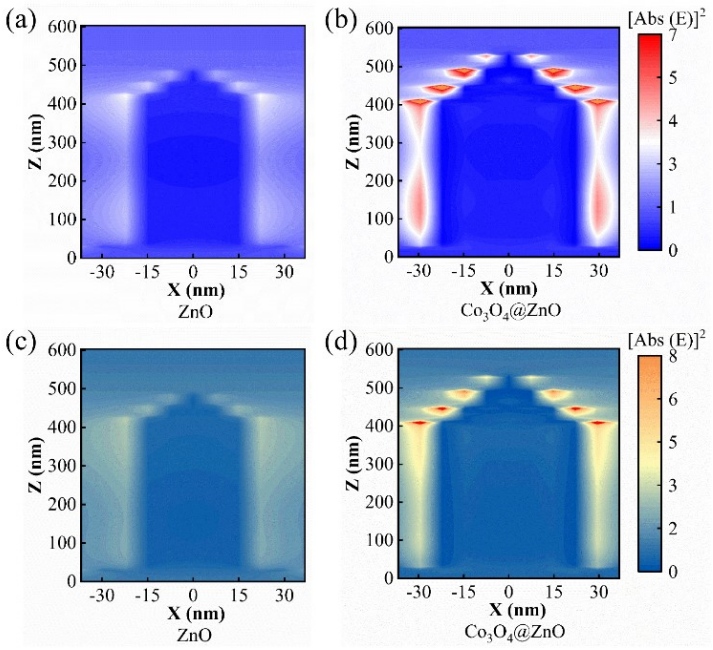

Fig. S14 The simulations of electric field distribution of ZnO and Co_3O_4@ZnO under light irradiation at (a, b) 550 nm and (c, d) 700 nm.

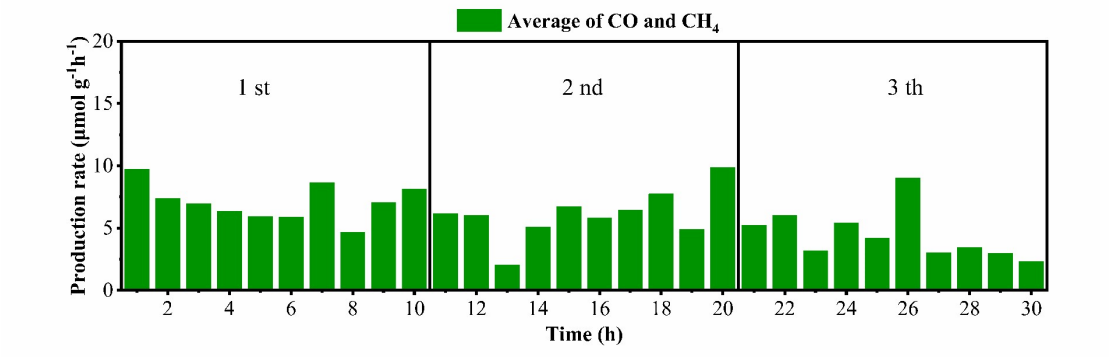

Fig. S15 The average production rate of CO and CH_4 every hour of Co_3O_4@ZnO in stability test.

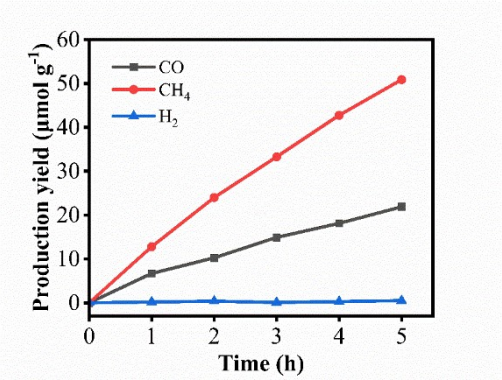

Fig. S16 Time-dependent performance of CO, CH_4 and H_2 yields of Co_3O_4@ZnO.

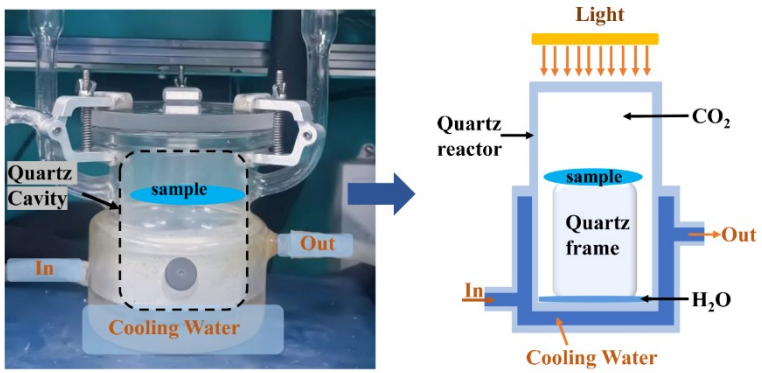

Fig. S17 The schematic diagram of reaction device for photocatalytic CO_2 reduction.

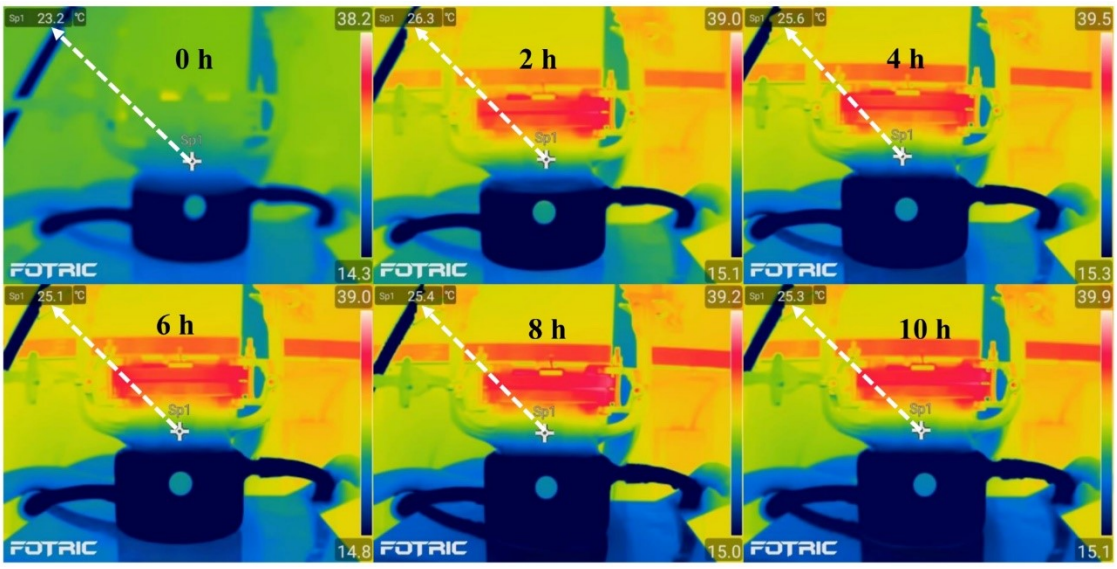

Fig. S18 The infrared images during the CO_2 photoreduction reaction.

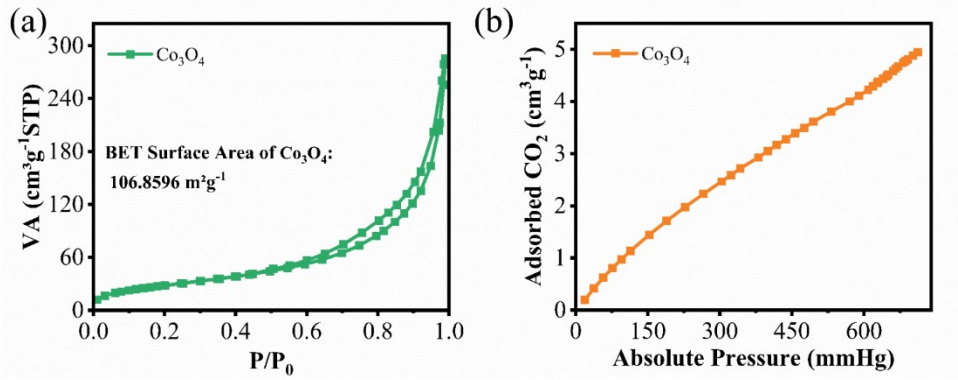

Fig. S19 (a) N_2 adsorption-desorption isotherm and (b) CO_2 adsorption isotherm of Co_3O_4.

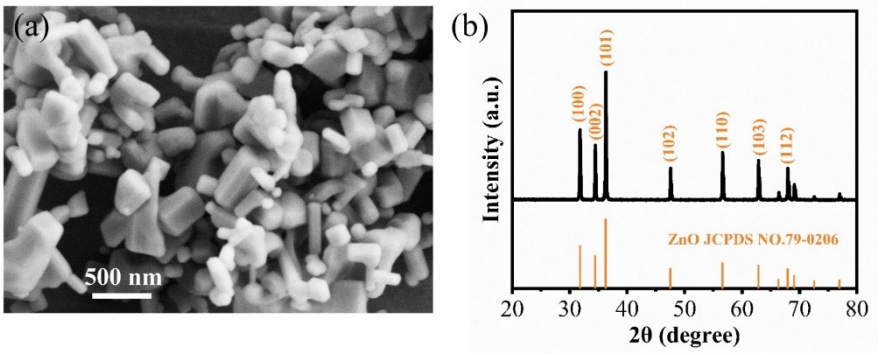

Fig. S20 (a) SEM image and (b) XRD pattern of raw material ZnO.

Synthesis of Co_3O_4:

The synthesis strategy of Co_3O_4 was similar to that of Co_3O_4@ZnO, except that solution A was absent. Specifically, the as-synthesized cobalt-based fragments were dispersed uniformly in an aqueous solution. The above system was then heated to 55°C for 30 min, followed by rapid cooling and collection of the reaction product. The precipitate was repeatedly washed with ethanol and deionized water. Finally, the product was dried at 80 °C for 48 h. The resulting sample was labeled Co_3O_4.

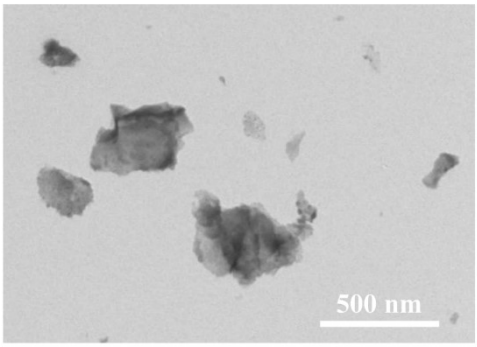

Fig. S21 TEM image of cobalt-based fragments.

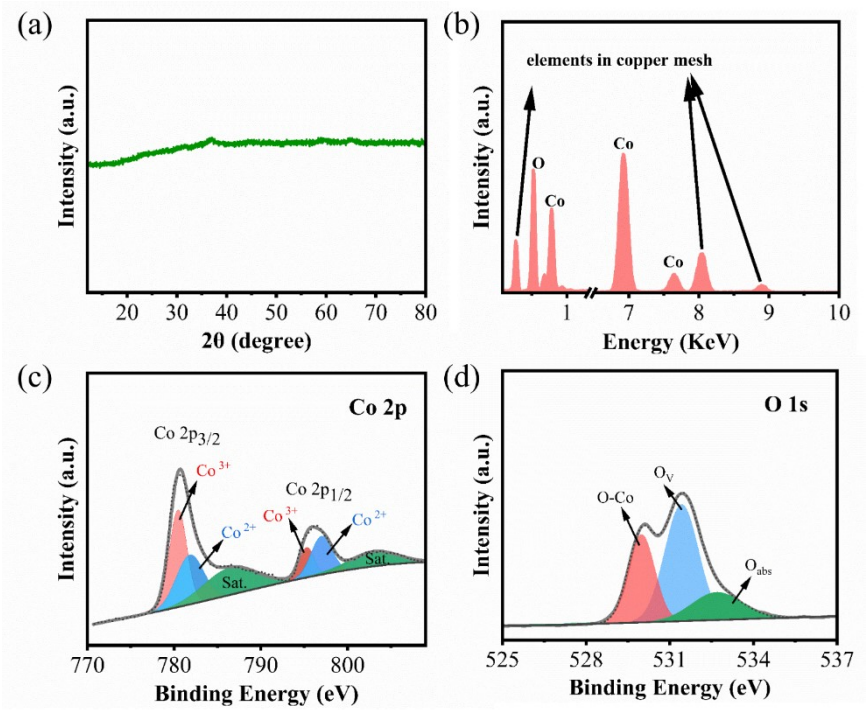

Fig. S22 (a) XRD pattern, (b) element energy spectrum of cobalt-based fragments. High-resolution XPS spectra of cobalt-based fragments: (c) Co 2p and (d) O 1s.

Cobalt based fragments exhibit poor crystallinity. Element energy spectrum shows that Co and O elements are included in the cobalt-based fragments. Combined with the results of high-resolution XPS spectra, it can be inferred that the cobalt-based fragments are poorly crystallized cobalt oxides. Co_3O_4 nanosheets were converted from cobalt-based fragments due to oxidation and recrystallization during the solvothermal reaction.

Quantum efficiency (QE) calculation:

QE (%) = (Number of effective electrons) / (Number of total photons) × 100% (S1)

Number of effective electrns = [2×r(CO)+8×r (CH_4)] × N_A = T-electrons × N_A (S2)

Number of total photons = (Light absorbed by the photocatalyst) × t / (Average photon energy) (S3)

light absorbed by the photocatalyst = $\boldsymbol{H} \times \boldsymbol{S}$ (S4)

Average photon energy = $\boldsymbol{hc}/\boldsymbol{\lambda}$ (S5)

QE (%) = (T-electrons × N_A × $\boldsymbol{hc}$) / ($\boldsymbol{H} \times \boldsymbol{S} \times t \times \boldsymbol{\lambda}$) (S6)

Where r(CO) and r(CH_4) is the generation rates of CO and CH_4 for photocatalyst, respectively. N_A is Avogadro's constant ($N_A = 6.022\times10^{23}$ mol^{-1}). $\boldsymbol{h}$ is Planck's constant ($\boldsymbol{h} = 6.63\times10^{-34}$ J·s). $\boldsymbol{H}$ represents the light input, which is 230 mW·cm^{-2} detected by the light power meter. t = 3600 s, and $\boldsymbol{c} = 3\times10^{8}$ m·s^{-1}. $\boldsymbol{S}$ is the irradiation area of the photocatalyst placed on the quartz plate inside the reactor ($\boldsymbol{S}$ = 28.26 cm^2).

The T-electrons of ZnO, Co_3O_4, 0.3-Co_3O_4-@ZnO, 0.6-Co_3O_4-@ZnO, and 0.9-Co_3O_4@ZnO are 2.44, 9.16, 57.4, 89.26, 61.82 μmol g^{-1} h^{-1} respectively. So the corresponding QE is calculated to be 0.0025%, 0.0094%, 0.0588%, 0.0914%, 0.0633%, respectively.

Table S1 The mass proportion of Zn and Co elements in the three different Co_3O_4@ZnO heterojunctions

Sample ID	**w_{Co} (mg L^{-1})**	**w_{Zn} (mg L^{-1})**

0.3-Co_3O_4@ZnO	0.772	32.66
0.6-Co_3O_4@ZnO	2.941	36.31
0.9-Co_3O_4@ZnO	5.069	35.683

Mass proportion of Co_3O_4 in Co_3O_4@ZnO composites = $w(Co_3O_4) / [w(Co_3O_4) + w(ZnO)]$ (S7)

$w(Co_3O_4) = n(Co_3O_4) \times M(Co_3O_4)$ (S8)

$w(ZnO) = n(ZnO) \times M(ZnO)$ (S9)

For Co_3O_4, $n(Co_3O_4) = n(Co) /3$ (S10)

For ZnO, n(ZnO) = n(Zn) (S11)

n(x) = w(x) / M (x), (x = Co, Zn, Co_3O_4, and ZnO) (S12)

So $w(Co_3O_4) = w(Co) \times M(Co_3O_4) / [3 \times M(Co)]$ (S13)

$w(ZnO) = w(Zn) \times M(ZnO) / M(Zn)$ (S14)

Where w(x), n(x), and M(x) is the wight, amount of substance, and molar mass of x (x= Co, Zn, Co_3O_4, and ZnO), respectively. The M(Co), M(Zn), $M(Co_3O_4)$ and M(ZnO) is 58.93, 65.93, 240.79, and 81.39 g mol^{-1}, respectively.

For 0.3-Co_3O_4@ZnO, w(Co) and w(Zn) is 0.772 and 32.66 mg L^{-1}, respectively. According to the eq S7, S13 and S14, mass proportion of Co_3O_4 in 0.3-Co_3O_4@ZnO is calculated to be 2.5%. Similarly, the mass proportion of Co_3O_4 in 0.6-Co_3O_4@ZnO and 0.9-Co_3O_4@ZnO is 8.1% and 13.5%, respectively.

Table S2 The comparison of CO_2 reduction performance of photocatalysts in this work and recently reported literatures

Photocatalyst	**Light**	**Reaction system**	**T-electrons**	**CH_4**	**Ref.**

	source		**rates [a] (μmol g^{-1} h^{-1})**	**selectivity [b] and stability**	
Co_3O_4@ZnO	300W Xe lamp (AM 1.5)	H_2O (2 mL), CO_2 (88 kPa)	89.26 (CO:4.23 CH_4:10.1)	70.5% 30 h	This work
Porous ZnO with exposed (110) facets	300W Xe lamp	Na_2SO_3 (0.25 M) and NaOH (1 M) saturated CO_2	1.912 (CO:0.76 CH_4:0.049)	11.0% 8 h	1
ZnO/$ZnMn_2O_4$ heterojunction	300W Xe lamp	$NaHCO_3$ (0.12 g) and H_2SO_4 (0.25 mL, 2 M)	8.74 (CO: 3.251 CH_4:0.275)	7.9% 24 h	2
ZnO/g-C_3N_4 heterojunction	UVC lamp with maximum length of 254 nm	H_2O (100 mL)	10.16 (CO: 2.1 CH_4: 0.745)	26.2% 6 h	3
ZnO nanoplates with defects	300W Xe lamp	Na_2SO_3 (100 mL, 0.25 M) and NaOH (1M) saturated CO_2	1.9 (CO: 0.95)	- 4 h	4
CdS/ZnO heterojunction	Visible light (λ > 400 nm)	H_2O (10 mL), CO_2 (0.4 MPa)	7.8 (CO: 3.9)	- 8 h	5
100Cu_2O-0.1Pd	300W Xe lamp (420-filter)	Na_2SO_3 (0.01 M), CO_2 (0.4 MPa)	0.26 (CO: 0.13)	- 8 h	6
TiO_2/$CsPbBr_3$ heterojunction	300 W Xe lamp	H_2O (100 μL), CO_2 (80 kPa), acetonitrile (30 mL)	18.04 (CO: 9.02)	- 16 h	7
AuNPs@SCX4$^+$	300 W Xe lamp (AM 1.5)	$NaHCO_3$ (84 mg) and H_2SO_4 (0.25 mL, 2 M)	3.37 (CO:1.685)	- 16 h	8
CdS/N-doped graphene	350 W Xe lamp (420-filter)	H_2SO_4 solution (0.3mL, 2M), $NaHCO_3$ (84 mg)	7.6 (CO: 2.6 CH_4:0.3)	10.3% 12 h	9
Porous Co_3O_4	LED lamp	Acetonitrile / H_2O mixture, TEOA as the electron donor and $[Ru(bpy)_3]Cl_2·6H_2O$ as photo-sensitizer	9.04 (CO: 4.52)	- 30 h	10
Phosphate modified-CeO_2/g-C_3N_4 heterojunction	300 W Xe lamp	H_2O (5 mL), CO_2 (4 bar)	1.04 (CO: 0.52)	- 24 h	11

$ZnIn_2S_4/BiVO_4$ heterojunction	300 W Xe lamp	H_2O (0.4 mL), CO_2 (1 atm)	11.7 (CO: 4.75 CH_4: 0.275)	5.5% 5 h	12
CeO_2/CuS heterojunction	300 W Xe lamp	H_2O, CO_2	8.48 (CO:4.24)	- 4 h	13
Ag-Cu_2O/ZnO heterojunction	300 W Xe lamp	H_2O (0.5 mL), CO_2 (1 atm)	6.72 (CO: 3.36)	- 16 h	14
Ti_3C_2/g-C_3N_4	300 W Xe lamp (420-filter)	H_2O, CO_2	6.6 (CO: 2.8 CH_4: 0.125)	4.3% 25 h	15

[a] T-electrons rates = 2r(CO) + 8r(CH_4), where r(CH_4) and r(CO) are the generated rates of CH_4 and CO, respectively.

[b] CH_4 selectivity (%) = r(CH_4) / [r (CO)+ r(CH_4)] × 100%.

References

1. P. Li, H. Hu, G. Luo, S. Zhu, L. Guo, P. Qu, Q. Shen and T. He, Crystal Facet-Dependent CO_2 Photoreduction over Porous ZnO Nanocatalysts, *ACS Appl. Mater. Interfaces*, 2020, **12**, 56039-56048.
2. H. Deng, X. Fei, Y. Yang, J. Fan, J. Yu, B. Cheng and L. Zhang, S-scheme heterojunction based on p-type $ZnMn_2O_4$ and n-type ZnO with improved photocatalytic CO_2 reduction activity, *Chem. Eng. J.*, 2020, **409**, 127377.
3. N. de Jesus Martins, I. C. H. Gomes, G. T. S. T. da Silva, J. A. Torres, W. Avansi, C. Ribeiro, A. R. Malagutti and H. A. J. L. Mourão, Facile preparation of ZnO:g-C_3N_4 heterostructures and their application in amiloride photodegradation and CO_2 photoreduction, *J. Alloy. Compd.*, 2021, **856**, 156798.
4. P. Li, S. Zhu, H. Hu, L. Guo and T. He, Influence of defects in porous ZnO nanoplates on CO_2 photoreduction, *Catal. Today*, 2018, **335**, 300-305.
5. L. Zhang, L. Zhang, Y. Chen, Y. Zheng, J. Guo, S. Wan, S. Wang, C. K. Ngaw, J. Lin and Y. Wang, CdS/ZnO: A Multipronged Approach for Efficient Reduction of Carbon Dioxide under Visible Light Irradiation, *ACS Sustain. Chem. Eng.*, 2020, **8**, 5270-5277.
6. X. Zhang, X. Zhao, K. Chen, Y. Fan, S. Wei, W. Zhang, D. Han and L. Niu, Palladium-modified cuprous(I) oxide with {100} facets for photocatalytic CO_2 reduction, *Nanoscale*, 2021, **13**, 2883-2890.
7. F. Xu, K. Meng, B. Cheng, S. Wang, J. Xu and J. Yu, Unique S-scheme heterojunctions in self-assembled $TiO_2/CsPbBr_3$ hybrids for CO_2 photoreduction, *Nat. Commun.*, 2020, **11**, 4613.
8. T. Skorjanc, K. M. Kamal, A. Alkhoori, G. Mali, A. K. Mohammed, Z. Asfari, K. Polychronopoulou, B. Likozar, A. Trabolsi and D. Shetty, Polythiacalixarene-

Embedded Gold Nanoparticles for Visible-Light-Driven Photocatalytic CO_2 Reduction, *ACS Appl. Mater. Interfaces*, 2022, **14**, 30796-30801.

9. C. Bie, B. Zhu, F. Xu, L. Zhang and J. Yu, In Situ Grown Monolayer N-Doped Graphene on CdS Hollow Spheres with Seamless Contact for Photocatalytic CO_2 Reduction, *Adv. Mater.*, 2019, **31**, 1902868.
10. W. Chen, B. Han, C. Tian, X. Liu, S. Liang, H. Deng and Z. Lin, MOFs-derived ultrathin holey Co_3O_4 nanosheets for enhanced visible light CO_2 reduction, *Appl. Catal., B*, 2018, **244**, 996-1003.
11. W. Li, L. Jin, F. Gao, H. Wan, Y. Pu, X. Wei, C. Chen, W. Zou, C. Zhu and L. Dong, Advantageous roles of phosphate decorated octahedral CeO_2 {111}/g-C_3N_4 in boosting photocatalytic CO_2 reduction: Charge transfer bridge and Lewis basic site, *Appl. Catal., B*, 2021, **294,** 120257.
12. Q. Han, L. Li, W. Gao, Y. Shen, L. Wang, Y. Zhang, X. Wang, Q. Shen, Y. Xiong, Y. Zhou and Z. Zou, Elegant Construction of $ZnIn_2S_4/BiVO_4$ Hierarchical Heterostructures as Direct Z-Scheme Photocatalysts for Efficient CO_2 Photoreduction, *ACS Appl. Mater. Interfaces*, 2021, **13**, 15092-15100.
13. X. Li, M. Wang, R. Wang, M. Shen, P. Wu, Z. Fu, M. Zhu and L. Zhang, A distinctive semiconductor-metalloid heterojunction: unique electronic structure and enhanced CO_2 photoreduction activity, *J. Colloid Interface Sci.*, 2022, **615**, 821-830.
14. F. Zhang, Y.-H. Li, M.-Y. Qi, Z.-R. Tang and Y.-J. Xu, Boosting the activity and stability of Ag-Cu_2O/ZnO nanorods for photocatalytic CO_2 reduction, *Appl. Catal., B*, 2019, **268,** 118380.
15. H. Wang, Q. Tang and Z. Wu, Construction of Few-Layer Ti_3C_2 MXene and Boron-Doped g-C_3N_4 for Enhanced Photocatalytic CO_2 Reduction, *ACS Sustain. Chem. Eng.*, 2021, **9**, 8425-8434.